ELSEVIER

Thermochimica Acta 377 (2001) 173–182

thermochimica acta

www.elsevier.com/locate/tca

Simultaneous measurements of complex heat capacity and complex thermal conductivity by two-channel AC calorimeter

A.A. Minakov[a,*], S.A. Adamovsky[b], C. Schick[b]

[a]*General Physics Institute, R.A.S., Vavilov st. 38, 119991 Moscow, Russia*
[b]*Department of Physics, University of Rostock, Universitatsplatz 3, 18051 Rostock, Germany*

Received 2 November 2000; received in revised form 10 December 2000; accepted 13 December 2000

Abstract

The new capabilities of the advanced two-channel AC calorimetry, when working at frequencies above quasi-static limit, were shown. The idea of the method was to use the information about the phases and the amplitudes of the temperature oscillations on both sides of a plate-like sample for direct simultaneous determination of the complex heat capacity $\mathbf{C}(\omega)$ and the complex thermal conductivity $\lambda(\omega)$, when the thermal oscillations were measured on both sides of the sample. Therefore, the complete set of the complex thermal parameters can be measured in the same experiment. The method provides a possibility to answer the fundamental question about the value of imaginary part of the complex thermal conductivity. It was found, that the argument of the complex thermal conductivity is considerably small with respect to that of the complex heat capacity. Thus, at least within the error of the experiment the thermal conductivity at glass transition in glycerol can be considered as a real valued parameter. In spite of the strong frequency dependence of the complex heat capacity, no frequency dependency of the thermal conductivity was observed.

Keywords: AC calorimetry; Complex heat capacity; Thermal conductivity; Temperature modulation calorimetry; Glass transition

1. Introduction

Temperature-modulated calorimetry (TMC) [1–9] is widely used for the investigation of phase transitions in polymers. Frequency dependent complex heat capacity can be measured by TMC [6–21]. The measurements of the complex heat capacity as a function of temperature, frequency and time provide unique information on relaxation phenomena at glass transitions [8–16], as well as on melting and crystallization kinetics in polymers [16–21].

The general scheme of TMC is to supply an oscillating heat flow $P_0\cos(\omega t)$ to a sample and to measure temperature oscillations $T_0-\cos(\omega t+\varphi)$. The measured parameters, P_0, T_0, and φ, provide information about Re and Im parts of the sample's complex heat capacity $\mathbf{C}_s(\omega)=C_s'-\mathrm{i}C_s''$. Thermal oscillations in the sample must be quasi-static, i.e. homogeneous, otherwise the measured parameters, T_0 and φ, are dependent on the sample's thermal conductivity λ_s and thickness d_s. The requirement of quasi-static modulation impose the following limitation $f \ll \lambda_s V_s/C_s d_s^2$ on the appropriate frequency $f=\omega/2\pi$, where V_s and C_s, are the sample's

* Corresponding author. Tel.: +7-095-132-82-68; fax: +7-095-132-82-81.
E-mail address: minakov@nsc.gpi.ru (A.A. Minakov).

0040-6031/01/$ – see front matter
PII: S0040-6031(01)00552-4

volume and absolute heat capacity. Usually, the appropriate frequency range is restricted by ca. 0.1 Hz for materials with low thermal conductivity, ca. 0.1 W/K m, such as polymers.

Recently, the new capabilities of TMC, when working at frequencies above this limit, were demonstrated [18–20]. The idea of the method was to measure simultaneously sample's heat capacity and thermal conductivity. The oscillating heat flow was supplied to one side of a thin, ca. 0.3 mm, plate-like sample and the temperature oscillations were measured on the other side. The two parameters, C_s and λ_s, were determined from the two measured values, T_0 and φ, when the sample's heat capacity and thermal conductivity were real valued, i.e. at temperatures far from phase transitions. Thus, the thermal conductivity was measured outside the phase transition region. Then, the temperature dependence $\lambda_s(T)$ was extrapolated to the phase transition region and the complex heat capacity $\mathbf{C}_s(\omega, T)$ was determined [20]. It was assumed that the thermal conductivity was frequency independent or such dependence was relatively weak to be neglected. But it is still an open question if this assumption is generally true. There is an ongoing discussion whether or not the measured phase at the glass transition is due to the imaginary part of heat capacity or imaginary part of thermal conductivity [9,12,15]. Also for other transitions like melting of polymers, where a large phase shift can be detected, the behavior of the thermal conductivity is unknown.

The aim of this work is to further advance the TMC technique, for simultaneous measurements of complex heat capacity $\mathbf{C}_s(\omega)$ and complex thermal conductivity $\lambda_s(\omega)$ for low thermal conducting materials, ca. 0.1 W/K m. The idea of the method is to measure the temperature oscillations $T_{01} - \cos(\omega t + \varphi_1)$ and $T_{02} - \cos(\omega t + \varphi_2)$ on both sides of a plate-like sample. The amplitudes T_{01} and T_{02}, as well as the phases φ_1 and φ_2, can be used to obtain simultaneously the following four parameters, $\mathrm{Re}(\mathbf{C}_s)$, $\mathrm{Im}(\mathbf{C}_s)$, $\mathrm{Re}(\lambda_s)$ and $\mathrm{Im}(\lambda_s)$. The mathematical algorithm to do so is presented in the first part of this paper. In the next section we describe the construction of the advanced two-channel AC calorimeter and it's calibration procedure.

Next, we demonstrate the capabilities of this two-channel technique, when applied for simultaneous measurements of complex heat capacity and complex thermal conductivity of polymers in the glass transition region. We present experimental data obtained for the glass transition in glycerol, which was used as a test material for other temperature-modulated [8–11,22] and hot-wire [22,23] techniques. The glass transition in glycerol is strong enough for testing a new technique.

This work can be considered as a step forward to measurements of the complete set of complex thermal parameters in the same experiment. Thus, we did not focus our affords on the accurate calibration and precise determination of the parameters of the investigated materials. We rather focused on qualitative peculiarities of the technique and we tried to answer the question, is the imaginary part of the thermal conductivity considerable in the glass transition region or can it be neglected?

2. The method, general description

First we consider an ideal cylindrical system of four layers, a disk-shaped sample placed between two identical sapphire substrates and maintained on a disk-shaped holder, as shown in Fig. 1. All these layers are thin disks of the same face area S. A film heater and a sensor are sputtered on the faces of the first sapphire substrate, which is maintained on the holder. The heater is on the face attached to the sample and the sensor is on the opposite face attached to the holder. The second sensor is placed on the face of the second sapphire substrate on the side, which is opposite to the sample. We assume that heat capacities and thermal resistances of the film heater and of the sensors are negligibly small, as well as the thermal contact resistances between all layers compared to the thermal resistance of the sample. Thus, the system can be described by the following parameters, the heat capacities $\mathbf{C}_s$, C_h, C_0, the thermal conductivities λ_s, λ_h, λ_0, and the thickness d_s, d_h, d_0 of the sample, holder and each of the sapphire substrates, respectively. The system is placed into a thermostat. The thermal link between the system and the thermostat occurs through an ambient gas pumped down to 10–100 Pa. This thermal link is described by the parameter G, ca. 1 mW/K, depending on the ambient gas and the system dimensions.

The resistive film heater provide a uniform heat flow, with oscillating part of the heat flow rate $P = P_0$

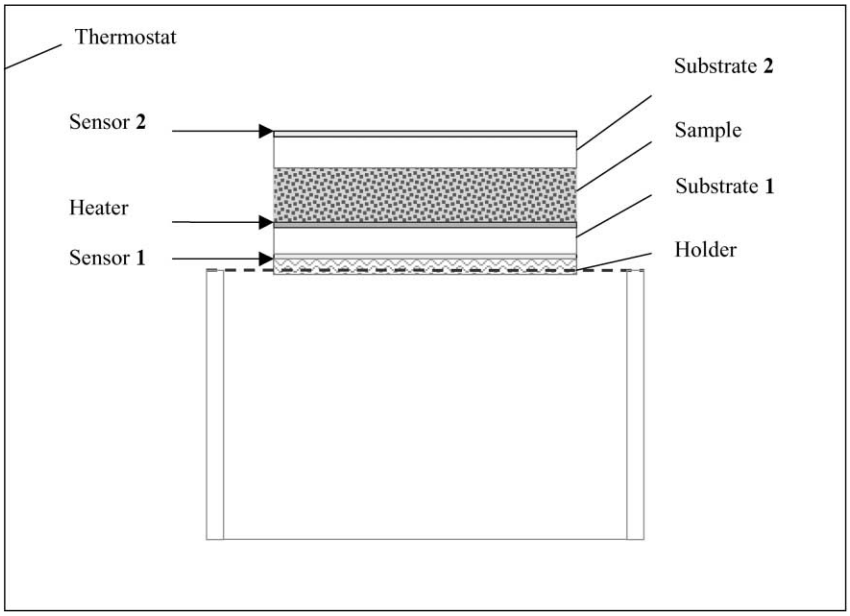

Fig. 1. Schematic cross-sectional view of the calorimeter cell. The sample is placed between two polished sapphire substrates. The heater and the first sensor, sensor 1, are sputtered on the first sapphire substrate. The second sensor, sensor 2, is sputtered on the top face of the second substrate. This sandwich is glued to a thin silk net, which serves as a holder. The cell is placed into the thermostat.

$\cos(\omega t)$. The heat flow is supplied to the sample's face connected with the first sapphire substrate at $z = 0$ and propagates through the system in both directions along the z-axis. The system thickness, ca. 0.5 mm, is considerably small with respect to diameter $D = 8$ mm. Therefore, the radial heat leakage through the periphery of the system can be neglected. Further we assume that the thermal oscillations are small enough to consider the linear-response approximation.

The plane thermal waves $\mathrm{Re}[\mathbf{T}_0 \exp(\mathrm{i}\omega t \pm \mathbf{k}_i z)]$ are exited in the ith layer, where $\mathbf{k}_i = \exp(\mathrm{i}\pi/4)\,(\omega \mathbf{c}_i/\lambda_i)^{1/2}$, $\mathbf{c}_i$ is complex specific heat capacity and λ_i the complex thermal conductivity of the ith layer material. Note, that the complex values are expressed in bold font and the modulus in italic: $\mathbf{c}_i = c_i \exp(-\mathrm{i}\phi_i)$, $\lambda_i = \lambda_i \exp(-\mathrm{i}\vartheta_i)$. The negative sings of the arguments of $\mathbf{c}_i$ and λ_i mean the delay in the system response. The stationary oscillating solution of the heat-transfer equation for the multilayered system can be described by the following relations

$$\mathbf{T}_i(t,z) = \exp(\mathrm{i}\omega t)\{\mathbf{a}_i \sinh[\mathbf{k}_i(z-\xi_i)] + \mathbf{b}_i \cosh[\mathbf{k}_i(z-\xi_i)]\},$$

where ξ_i is the coordinate of ith boundary. The complex coefficients $\mathbf{a}_i$ and $\mathbf{b}_i$ are determined by boundary conditions for the temperature and the heat flow amplitudes on the faces of the ith layer. The general solution for the multilayered system of n layers was received in [18,20]. We use this solution for calculations of the thermal oscillations in the system described above.

Denote the effective heat capacities $\mathbf{C}_1 = P_0/(\mathrm{i}\omega \mathbf{T}_{01})$ and $\mathbf{C}_2 = P_0/(\mathrm{i}\omega \mathbf{T}_{02})$ related to the amplitudes $\mathbf{T}_{01}$ and $\mathbf{T}_{02}$ of the temperature oscillations measured by the first and the second sensor of the system shown in Fig. 1. Then, the effective heat capacities $\mathbf{C}_1$ and $\mathbf{C}_2$ can be expressed as follows

$$\mathbf{C}_1 = \cosh(\alpha_0)\frac{\mathbf{B}_1 + \mathbf{B}_3 + G/\mathrm{i}\omega}{1 + \mathbf{b}_\mathrm{s}} \tag{1}$$

$$\mathbf{C}_2 = \cosh(\alpha_0)\cosh(\alpha_\mathrm{s})\frac{\mathbf{B}_1 + \mathbf{B}_3 + G/\mathrm{i}\omega}{1 + \mathbf{b}_\mathrm{h}} \tag{2}$$

where $\alpha_l = d_l \mathbf{k}_l$ is the parameter characterizing the thermal thickness of the lth layer. Denote complex functions $\mathbf{Y}_l(\alpha_l) = \tanh(\alpha_l)/\alpha_l$. Then, the terms $\mathbf{B}_1$,

$\mathbf{B}_3$, $\mathbf{b}_s$ and $\mathbf{b}_h$ can be written as functions of the sample's parameters $\mathbf{C}_s$ and α_s as follows

$$\mathbf{B}_1 = 2\mathbf{C}_0\mathbf{Y}_0 + \mathbf{C}_h\mathbf{Y}_h + \mathbf{C}_s\mathbf{Y}_s,$$

$$\mathbf{B}_3 = C_h\left(\frac{i\omega\mathbf{C}_s/K_0 + \alpha_s^2 C_0}{\mathbf{C}_s}\right)\mathbf{Y}_0\mathbf{Y}_h\mathbf{Y}_s + C_0\left(\frac{i\omega C_h\mathbf{Y}_h}{K_0} + \frac{\mathbf{Y}_s\alpha_s^2 C_0}{\mathbf{C}_s}\right)\mathbf{Y}_0^2,$$

$$\mathbf{b}_s = \left(\frac{\alpha_s^2 C_0}{\mathbf{C}_s}\right)\mathbf{Y}_0\mathbf{Y}_s, \qquad \mathbf{b}_h = \left(\frac{i\omega C_h}{K_0}\right)\mathbf{Y}_0\mathbf{Y}_h, \tag{3}$$

where $K_0 = S\lambda_0/d_0$ is the thermal conductance of each sapphire substrate. Note, that dimensionless parameter α_l is proportional to $\sqrt{\omega}$ and $\alpha_l \ll 1$ at sufficiently low frequencies. Thus, at low frequencies $\tanh(\alpha_l) \approx \alpha_l$ and $\mathbf{Y}_l(\alpha_l) \approx 1$. Of course, in the low frequency limit the obvious relation $\mathbf{C}_1 = \mathbf{C}_2 = (2C_0 + C_h + \mathbf{C}_s + G/i\omega)$ follows from Eqs. (1) and (2). The term $G/i\omega$ describes the heat leakage from the system to the thermostat during oscillation period. At sufficiently small heat leakage from the system to the thermostat the effective heat capacities $\mathbf{C}_1$ and $\mathbf{C}_2$ are equal simply to the total heat capacity of the system $\mathbf{C}_t = 2C_0 + C_h + \mathbf{C}_s$.

In general, the two complex parameters $\mathbf{C}_s$ and α_s can be determined from the measured $\mathbf{C}_1$ and $\mathbf{C}_2$, provided other parameters of Eqs. (1) and (2) are measured in advance. Finally, the parameter λ_s can be determined from the following relation, $\lambda_s = (i\omega/\alpha_s^2)\mathbf{C}_s d_s/S$. When the sample's face area S_s is not exactly equal to S the relation should be corrected as follows

$$\lambda_s = \left(\frac{i\omega}{\alpha_s^2}\right)\frac{\mathbf{C}_s d_s}{S_s} \tag{4}$$

The sample's face area S_s equals V_s/d_s, where the sample's thickness d_s is fixed by the calibrated spacers as described below. The sample's volume V_s can be estimated from the sample's mass for the solid samples or directly measured as described below for the liquid samples.

3. Two-channel AC calorimeter

The construction of the calorimeter was described in [24,25]. The calorimeter cell, the system for creation and registration of temperature oscillations in a disk-shaped sample, consists of a heater, a sensor, and a holder. The scheme of this system is shown in Fig. 1. The heater and the sensors are formed on the surfaces of sapphire disks of 8 mm diameter and of thickness 0.15 mm. The heater is a chromium film, sputtered on the polished face of the sapphire substrate. Copper contact pads are sputtered on the chromium film, and copper wires of 50 μm diameter are welded to the pads. The power of this resistive heater equals $P_0(1 + \cos\omega t)$, where $\omega/2$ is the angular frequency of the electric current and P_0 is the average power of the heater. To form the sensor, a copper field is sputtered on the opposite also polished face of the sapphire substrate. The thermocouple (Cu–Constantan) wires of 50 μm diameter are welded to the copper field. The system is glued on a thin silk net, which serves as a holder. The appropriate model of the holder is a disk of 8 mm diameter consisting of glue and silk net. Thus, the cell consists of four layers, including sample. The heat capacities of wires, film-heater and sensors are negligibly small. We assume that the heat leakage though the wires can also be neglected as it was shown in [25] for analogous cell with the same wires and sapphire substrates of 3 mm diameter.

The sample was placed between the polished sapphire substrates, without any pan. The distance between the substrates was fixed by two glass fibers of ca. 0.3 mm diameter placed between the sapphire substrates. This sandwich was pressed with a thin silk thread. The shape of the liquid sample was stable due to the surface tension force.

The ideal thermal contact of the sample with the polished sapphire substrates was assumed. This approximation is sufficient for polymers, the materials with relatively low thermal conductivity, $\lambda_s < 1$ W/K m, as it was shown in [26]. The thermal contact between substrates and glycerol was sufficiently good and stable due to good adhesion with the substrates. In the case of solid samples, on the other hand, the thermal contact should be formed by a liquid-like material. The thermal conductance of a dry thermal contact is relatively low, unstable and irreproducible. Thus, when dealing with solids, an appropriate thermal contact can be made by means of a thin, ca. 5 μm, layer of a lubricant between sample and substrate. The vacuum grease, Apiezon™, can be used for a good, reproducible and stable thermal contact, as it was

shown in [26]. When the thermal contact resistance can not be neglected, it can be taken into account as it was shown in [26]. In this case, the information from the measurements with a reference sample or with the same sample at temperatures far from the phase transition are required.

The cell construction presented in this paper had the following disadvantage. The wire-leads of the heater were placed in the sample's region in the periphery of the first sapphire substrate. The sample was placed between these leads and was in thermal contact with the substrates. It was not possible to set the substrates in close connection, when the sample was removed from the cell, i.e. there was no direct thermal contact between the substrates of the empty cell. Thus, the empty cell calibration could not be performed. To avoid this disadvantage we plan to produce in nearest future a cell with the heater placed on the outer face of the second substrate. Then, the heater and one of the sensors will be on the same face separated by a dielectric layer of SiO_2 between these two metallic layers. There will be no wires in the sample's region and the empty cell calibration will be possible.

In the present work the calibration was performed with two other cells, A and B, which were made almost the same as the previous one. These cells were made with only one sensor and a heater. The heater and the sensor were placed on the faces out of the sample's region. The results of the measurements of the thermal parameters of these cells were averaged and used as calibration parameters for the cell with two sensors. The total heat capacities of the cells A and B were the same within 14%. The total substrates mass of the cell A was by 6% smaller than that of the cell B. The total substrates mass of the cell with two sensors was intermediate. Thus, we suppose that the total heat capacity of the cell with two sensors was also intermediate and coincided with the average parameter within 7%. For the cells A and B the parameters $2C_0$, C_h, $2\alpha_0/\sqrt{f}$, $\alpha_h/\sqrt{f}$, and G were measured in the temperature range 150–350 K in the frequency range 0.02–100 Hz. These parameters were frequency independent within 3% accuracy. The results for the cells at 150 and 300 K are presented in Table 1.

This is only the parameter G, which depends on ambient gas pressure. But this dependence is very weak in the pressure range 1–100 Pa. In all measurements the nitrogen gas pressure was ca. 10–100 Pa and G was varied in the range 1.6–3.6 mW/K, when the temperature was changed from 150 to 350 K.

Once the cell calibration is performed, the described algorithm makes it possible to carry out simultaneous measurements of the sample's heat capacity and thermal conductivity. The sample's parameters, $\mathbf{C}_s$ and λ_s, can be determined from the measured, $\mathbf{C}_1$ and $\mathbf{C}_2$, according to Eqs. (1) and (2). Actually, the amplitudes $T_{0i} = P_0/(\omega\mathbf{C}_i)$ and the phase shifts $\psi_i = \arg(1/\mathbf{C}_i)$ between the temperature oscillations in the heater and in the ith sensor are measured by a lock-in amplifier. Of course, for simultaneous measurements of both T_{01} and T_{02}, as well as of ψ_1 and ψ_2, two lock-in amplifiers are required. This requirement is essential, when irreproducible thermal-history and time dependent melting-crystallization process are investigated. On the other hand, when reproducible processes, like glass transition, are studied, only one lock-in amplifier can be used for successive measurements of the temperature oscillations in both sensors.

To focus on complex heat capacity and thermal conductivity, we consider the frequency domain 0.02–

Table 1
Thermal parameters of two cells, A and B, at temperatures 150 and 300 K[a]

Cell	Temperature (K)	Heat capacity (mJ K^{-1})			$\alpha/\sqrt{f}$ ($s^{1/2}$)		G (mW K^{-1})
		Two substrates	Holder	Total	Two substrates	Holder	
A	150	19.5	3.3	22.8	0.082	2.48	1.61
	300	52.9	4.4	57.3	0.276	2.40	3.29
B	150	21.0	5.4	26.4	0.078	3.39	1.70
	300	55.0	9.0	64.0	0.243	2.87	3.42

[a] $\alpha = kd$: the dimensionless parameter characterizing thermal thickness of a layer of thickness d, where $k = (\omega c/\lambda)^{1/2}$; G: parameter characterizing thermal link between the system and thermostat.

10 Hz appropriate for these measurements with sample of thickness ca. 0.3 mm.

Finally, the temperature gradient across the sample can be estimated from the following relation, $\Delta T_s/d_s = P_0/2S\lambda_s$. The measurements were performed at the amplitude of the heat-flow rate $P_0 = 25$ mW, d_s ca. 0.3 mm, S_s ca. 40 mm^2, and λ_s ca. 0.3 W/K m. Thus, the temperature difference across the sample, ΔT_s ca. 0.03 K, was not essential.

4. Experimental results and discussion

Next we apply the method to studying glass transition in glycerol, $C_3H_8O_3$, which is a liquid with density ca. 1.26 g/cm^3 and molecular weight $M = 92.1$ Da. Glycerol is a hydroscopic material and the samples always contain some amount of water. The glass transition studies in glycerol samples with 0.1 and 1% of H_2O yielded identical results [23]. Moreover, the study of glass transition in 75% (v/v) glycerol-water mixture showed that the qualitative behavior of this transition was the same in the mixture as in the pure glycerol [27]. As we were interested in the qualitative features of the glass transition in glycerol, we were not interested in the water impurity contamination in the sample studied. The sample was received from commercial medical shop and was stored in the closed vessel before measurements.

A glycerol drop of calibrated volume, ca. 12.0 ± 0.5 mm^3, was placed between sapphire substrates. The distance between the substrates was fixed by two fiberglass cylinders of 0.33 ± 0.01 mm diameter. Thus, the thickness and the face area of the sample were equal to 0.33 ± 0.01 and 36 ± 2 mm^2, respectively. The sample was supercooled below glass transition with the cooling rate ca. 10 K/min. Then, the ambient gas was pumped down to 100 Pa. Next, the heating-cooling cycling of 1 K/min rate were proceeded at the same pressure in the temperature range 160–220 K.

After the first heating-cooling cycle the results of $C_1(T)$ and $C_2(T)$ measurements were reproducible and were the same at cooling and heating, i.e. no hysteresis was observed. The temperature dependences of the absolute values C_1 and C_2, as well as of the phase shifts $\psi_1 = \arg(1/\mathbf{C}_1)$ and $\psi_2 = \arg(1/\mathbf{C}_2)$, measured

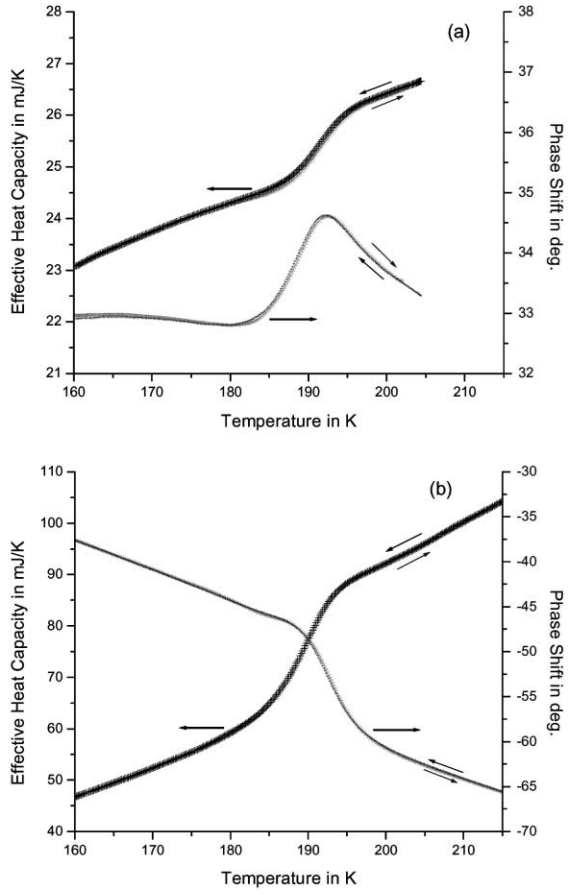

Fig. 2. Temperature dependences of (a) the effective heat capacity C_1 and the phase shift $\psi_1 = \arg(1/\mathbf{C}_1)$ measured by the sensor 1, as well as of (b) the effective heat capacity C_2 and the phase shift $\psi_2 = \arg(1/\mathbf{C}_2)$ measured by the sensor 2, for glycerol sample of 0.33 mm thickness and 12 mm^3 volume. The experiment was performed at underlying heating-cooling rate ca. 1 K/min, the modulation frequency $f = 0.5$ Hz and the heat-flow rate amplitude $P_0 = 25$ mW. The amplitude of the temperature oscillations was ca. 0.3 K in the sensor 1 and ca. 0.1 K in the sensor 2.

by the sensor 1 and the sensor 2 are shown in Fig. 2(a) and (b). The experiment was performed at the modulation frequency $f = 0.5$ Hz, the heat-flow rate $P_0 = 25$ mW and the temperature modulation amplitudes ca. 0.3 K in the sensor 1 and ca. 0.1 K in the sensor 2. To prevent crystallization between measurements the sample was kept below glass transition at 150 K. Well defined glass transition was observed, when temperature oscillations were measured in both sensors. The amplitude T_{01} of the thermal modulation

in the first sensor, close to the heater, was ca. three times larger than T_{02}. Thus, the effective heat capacity C_1 was ca. three times smaller than C_2. The steps in $C_1(T)$ and $C_2(T)$ were related to the step in $\mathbf{C}_s(T)$ at glass transition. The phase shift ψ_1 in the first sensor, close to the heater, was positive (because, $\psi_1 = \varphi_1 + \pi/2$). The well defined peak at the glass transition in $\psi_1(T)$ is related to the peak of $\mathrm{Im}(\mathbf{C}_s(T))$. On the other hand, the phase shift ψ_2 was negative due to the phase lag of the thermal wave transmitted through the sample. This phase lag was related to the thermal-thickness parameter of the sample α_s, which is proportional to the square root of the ratio C_s/λ_s. Thus, the phase shift ψ_2 was more and more negative with increasing the sample's heat capacity and with decreasing the thermal conductivity at heating. The step in the dependence $\psi_2(T)$ was related to the step in $C_s(T)$. Nevertheless, this step was shifted with respect to the step in $C_s(T)$ due to the peak in the temperature dependence of $\mathrm{Im}(\mathbf{C}_s)$.

The frequency dependences of the thermal parameters, $\mathbf{C}_s$ and λ_s, were measured at different temperatures in the range 160–220 K. Consider these dependences below glass transition. As shown in Fig. 3 the experimental data $C_1(f)$ and $C_2(f)$, as well as $\psi_1(f)$ and $\psi_2(f)$, at 160K are well described by Eqs. (1) and (2) with real valued $C_s = 14.7$ J/K and $\lambda_s = 0.32$ W/K m in the frequency range 0.04–10 Hz. These values, $C_s(160\ \mathrm{K})$ and $\lambda_s(160\ \mathrm{K})$, were frequency independent within 7% accuracy. It is noteworthy, that the error of the cell calibration could lead to the inaccuracy ca. 7% in the measured frequency dependences of C_s and λ_s. Thus, the measured parameters were frequency independent within the error of the experiment at 160 K in the range 0.04–10 Hz. Analogous results were obtained at the relatively high temperature 220 K.

In the temperature range 180–205 K and frequency domain 0.04–10 Hz the heat capacity $\mathbf{C}_s$ was complex and frequency dependent as shown in Fig. 4. These are the curves, $\mathrm{Re}(\mathbf{C}_s(f))$ and $\mathrm{Im}(\mathbf{C}_s(f))$, typical for the relaxation process at a glass transition. The frequency dependences of $\mathrm{Re}(\mathbf{C}_s)$ and $\mathrm{Im}(\mathbf{C}_s)$ were in agreement with results from heat capacity spectroscopy [8–11] and dielectric spectroscopy [27–31] of glycerol. The observed glass transition temperatures, $T_g(f)$ shown in Fig. 5, were about 5 K below the values reported in [8–11,28–30]. The glass transition at temperature $T_g(0.5\ \mathrm{Hz}) \approx 195$ K measured in [31], for 99.5% pure glycerol, was close to the results of our experiments $T_g(0.4\ \mathrm{Hz}) \approx 194$ K.

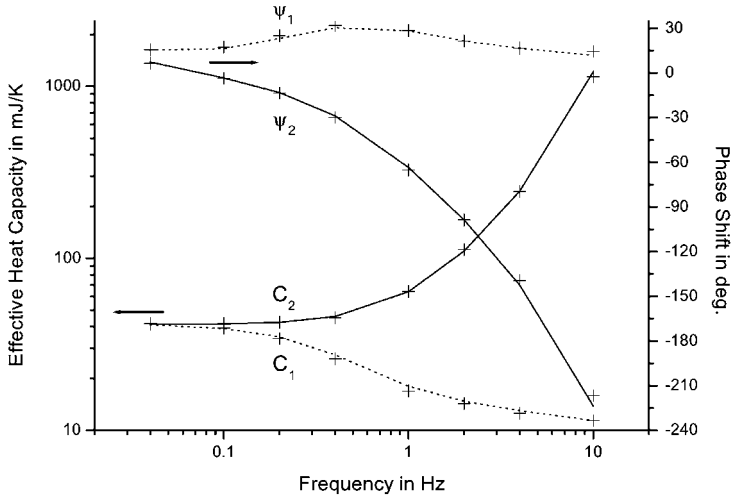

Fig. 3. Frequency dependences of measured (crosses) and calculated (line) effective heat capacity C_1 and phase shift ψ_1 (dot line), as well as of C_2 and ψ_2 (solid line) for glycerol sample the same as in Fig. 2. The experiment was performed at 160 K and at heat-flow rate amplitude $P_0 = 25$ mW. The temperature modulation amplitude was ca. 1.5–0.01 K in the sensor 1 and ca. 1.5–0.001 K in the sensor 2, when the frequency was changed in the range 0.04–10 Hz.

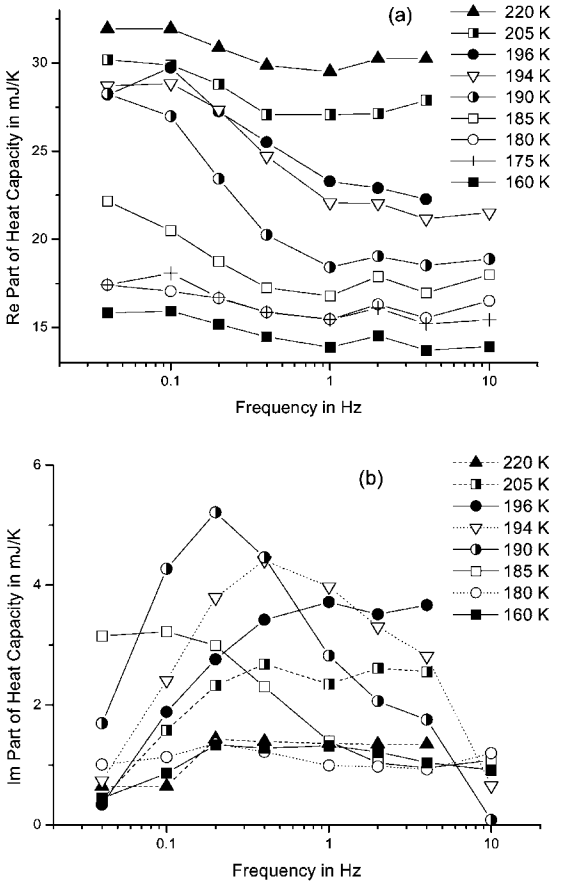

Fig. 4. Frequency dependences of Re($\mathbf{C}_s$) and Im($\mathbf{C}_s$) at different temperatures in the glass transition region measured for the same glycerol sample as in Fig. 2. The experiments were performed at the same conditions as in Fig. 3.

The strong, ca. 30%, frequency dependence of the complex heat capacity is shown in Fig. 4. On the other hand, no considerable Im part of the thermal conductivity was observed. The temperature dependences of the arguments ϕ and ϑ of the complex heat capacity $C_s \exp(-i\phi)$ and the complex thermal conductivity $\lambda_s \exp(-i\vartheta)$ at 0.2 Hz are shown in Fig. 6. One can see a well-defined peak of $\phi(T)$. On the contrary, no considerable anomaly in $\vartheta(T)$ dependence was observed. The argument of the complex thermal conductivity is considerably small with respect to that of the complex heat capacity. The frequency dependence of the thermal conductivity was also below the error of the experiment. This is the error of the cell calibration, ca. 7%, which can lead to the same error in the

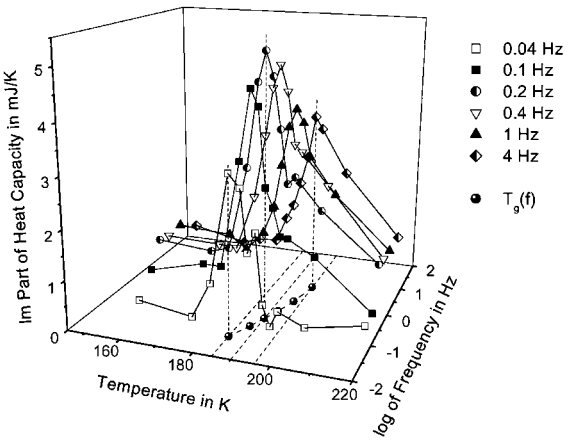

Fig. 5. The plot of Im($\mathbf{C}_s$) vs. T and f for the same conditions as in Fig. 4. The projections of the maxima of Im($\mathbf{C}_s(T)$) dependences on $T-f$ plane show the frequency dependence of the glass transition temperature $T_g(f)$.

frequency dependences of $\mathbf{C}_s$ and λ_s. It is noteworthy, that the error in the sample's geometrical parameters can lead only to a shift of the values $\mathbf{c}_s$ and λ_s calculated from the measured parameters $\mathbf{C}_s$ and α_s without changing the frequency dependences. Thus, the thermal conductivity of glycerol can be considered as a real valued and frequency independent parameter at least within the error of this experiment.

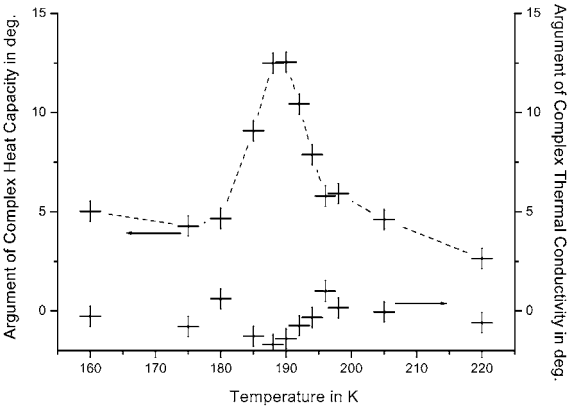

Fig. 6. Temperature dependences of the arguments ϕ and ϑ of the complex heat capacity $C_s \exp(-i\phi)$ and the complex thermal conductivity $\lambda_s \exp(-i\vartheta)$ of glycerol sample the same as in Fig. 2. The experiment was performed at the frequency 0.2 Hz, the heat-flow rate amplitude $P_0 = 25$ mW and the temperature modulation amplitudes ca. 0.45 K in the sensor 1 and ca. 0.25 K in the sensor 2.

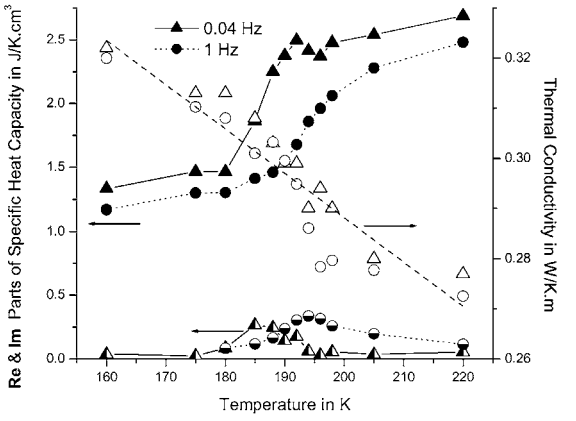

Fig. 7. Temperature dependences of Re and Im parts of the specific heat capacity $\boldsymbol{C}_s$, as well as of the thermal conductivity absolute value λ_s, of the same glycerol sample as in Fig. 2 at 0.04 and 1 Hz. The temperature modulation amplitudes were ca. 1.5 K in both sensors at 0.04 Hz, and ca. 0.2 K in the sensor 1 and ca. 0.025 K in the sensor 2 at 1 Hz.

Next, we consider the temperature dependence of the thermal conductivity absolute value λ_s. The temperature dependences $\lambda_s(T)$, as well as $\mathrm{Re}(\mathbf{c}_s(T))$ and $\mathrm{Im}(\mathbf{c}_s(T))$, are shown in Fig. 7. Well defined steps and maxima in $\mathrm{Re}(\mathbf{c}_s(T))$ and $\mathrm{Im}(\mathbf{c}_s(T))$, respectively, were observed at glass transition. These dependences were in agreement with the results of the heat capacity measurements presented in [32,33]. The values of the specific heat capacity below glass transition, ca. 1.25 ± 0.1 J/K cm^3, and above glass transition, ca. 2.5 ± 0.15 J/K cm^3, were in agreement within the experimental error with the values 0.85 J/K g, i.e. 1.1 J/K cm^3, and 1.9 J/K g, i.e. 2.4 J/K cm^3, presented in [32], provided the glycerol density was equal to 1.26 g/cm^3. The specific heat capacity step at glass transition, ca. 1.25 ± 0.15 J/K cm^3, is in agreement with the results presented in [33] for DCS measurements, 1.02 J/K g, i.e. 1.29 J/K cm^3, and for TMDSC measurements, 0.97 J/K g, i.e. 1.18 J/K cm^3.

An artificial peak in $\lambda_s(T)$ dependence can be observed at T_g due to the frequency dependence of $\mathbf{C}_s$. Such peak was observed for glycerol in [22,23]. As it was shown in [9,12] the apparent peak in $\lambda_s(T)$ was due to nonzero Im part of $\mathbf{C}_s$ which was neglected in the analysis of the experimental data in [22,23]. This anomaly disappears, when one takes into account nonzero Im part of heat capacity. On the other hand, an artificial anomaly in $\lambda_s(T)$ dependence can be observed due to the cell calibration inaccuracy. Because, the sample's heat capacity is extracted from the measured effective heat capacity by subtracting of the cell heat capacity. Then, the thermal conductivity is calculated from the extracted $\mathbf{C}_s$ and α_s according to Eq. (4). As shown in Fig. 7 we did not find any anomaly and frequency dependence of the thermal conductivity in glycerol at glass transition within the error of the experiment. Thermal conductivity was decreased from 0.32 ± 0.02 W/K m to 0.27 ± 0.02 W/K m in the temperature range 160–220 K. These results were in agreement with $\lambda_s(T)$ ca. 0.31–0.30 and 0.37–0.31 W/K m measured in the same temperature range in [23] and [9], respectively.

Thus, we can conclude that at least within the error of the experiment the thermal conductivity at glass transition in glycerol is a real valued parameter in spite of the strong, ca. 30%, frequency dependence of the complex heat capacity.

5. Conclusions

The advanced two-channel AC calorimetry, when working at frequencies above the quasi-static limit, can be applied for simultaneous measurements of complex heat capacity and complex thermal conductivity. Therefore, the complete set of the complex thermal parameters can be measured in the same experiment. The mathematical algorithm for such measurements is developed. This algorithm can be applied for different materials, when the complex amplitudes of the temperature modulations are measured on both sides of the sample. It is noteworthy, that this method of simultaneous measurements of the complex heat capacity and the complex thermal conductivity can provide important information not only at glass transition but also in the melting range of polymers. The method provides a possibility to answer the fundamental question about the value of Im part of the thermal conductivity. It was found, that the argument of the complex thermal conductivity is considerably small with respect to that of the complex heat capacity at glass transition in glycerol. At least within the error of the experiment the simultaneous and direct measurements show that the thermal conductivity can be considered as real valued parameter.

In spite of the strong, ca. 30%, frequency dependence of the complex heat capacity, no frequency dependency of the thermal conductivity was observed.

Acknowledgements

The financial support of the German Science Foundation, grant numbers SCHI 331/7-1 and 436 RUS 17/26/00, is gratefully acknowledged.

References

[1] Y.A. Kraftmakher, Zh. Prikl. Mekh. Tekh. Fiz. 5 (1962)176.
[2] P.F. Sullivan, G. Seidel, Phys. Rev. 173 (1968) 679.
[3] P. Handler, D.E. Mapother, M. Rayl, Phys. Rev. Lett. 19 (1967) 356.
[4] M.B. Salamon, Phys. Rev. B 2 (1970) 214.
[5] I. Hatta, A. Ikushima, J. Phys. Chem. Solids 34 (1973) 57.
[6] M. Reading, Trend Polym. Sci. 8 (1993) 248.
[7] B. Wunderlich, Y.M. Jin, A. Boller, Thermochim. Acta 238 (1994) 277.
[8] N.O. Birge, S.R. Nagel, Phys. Rev. Lett. 54 (1985) 2674.
[9] N.O. Birge, Phys. Rev. B 34 (1986) 1631.
[10] N.O. Birge, P.K. Dixon, N. Menon, Thermochim. Acta 304/305 (1997) 51.
[11] E. Donth, J. Korus, E. Hempel, M. Beiner, Thermochim. Acta 304/305 (1997) 239.
[12] Y.-H. Jeong, Thermochim. Acta 304/305 (1997) 67.
[13] J. Korus, M. Beiner, K. Busse, S. Kahle, R. Unger, E. Donth, Thermochim. Acta 304/305 (1997) 99.
[14] S. Weyer, A. Hensel, J. Korus, E. Donth, C. Schick, Thermochim. Acta 304/305 (1997) 251.
[15] Yu.I. Polikarpov, A.I. Slutsker, Thermochim. Acta 304/305 (1997) 277.
[16] G.W.H. Hohne, Thermochim. Acta 304/305 (1997) 209.
[17] J.E.K. Schawe, E. Bergmann, Thermochim. Acta 304/305 (1997) 179.
[18] A.A. Minakov, Yu.V. Bugoslavsky, C. Schick, Thermochim. Acta 317 (1998) 117.
[19] A.A. Minakov, C. Schick, Thermochimica Acta 330 (1999) 109.
[20] A.A. Minakov, Yu.V. Bugoslavsky, C. Schick, Thermochim. Acta 342 (1999) 7.
[21] C. Schick, M. Merzlyakov, A. Minakov, A. Wurm, J. Therm. Anal. Calorim. 59 (2000) 279.
[22] D.G. Cahill, R.O. Pohl, Phys. Rev. B 35 (1987) 4067.
[23] O. Sandberg, P. Andersson, G. Backstrom, J. Phys. E: Scientific Instruments 10 (1977) 474.
[24] A.A. Minakov, O.V. Ershov, Cryogenics (ICEC Suppl.) 34 (1994) 461.
[25] A.A. Minakov, Thermochim. Acta 304/305 (1997) 165.
[26] A.A. Minakov, Thermochim. Acta 345 (2000) 3.
[27] M. Settles, F. Post, D. Muller, A. Schulte, W. Doster, Biophysical Chem. 43 (1992) 107.
[28] K.L. Ngai, R.W. Rendell, Phys. Rev. B 41 (1989) 754.
[29] C. Hansen, R. Richert, J. Phys.: Condens. Matter. 9 (1997) 9661.
[30] N. Menon, K.P. O'Brien, P.K. Dixon, L. Wu, S.R. Nagel, J. Non-Cryst. Solids 141 (1992) 61.
[31] B. Schiener, B.V. Chamberlin, G. Diezemann, R. Bohmer, J. Chem. Phys. 107 (1997) 7746.
[32] P. Claudy, J.C. Commercon, J.M. Letoffe, Thermochim. Acta 128 (1988) 251.
[33] E. Hempel, G. Hempel, A. Hensel, C. Schick, E. Donth, J. Phys. Chemistry B 104 (2000) 2460.